UC Riverside

UC Riverside Previously Published Works

Title

Evaluating soil nitrate dynamics in an intercropping dripped ecosystem using HYDRUS-2D

Permalink

https://escholarship.org/uc/item/2mp4d0c5

Authors

Chen, Ning

Li, Xianyue

Šimůnek, Jirí

et al.

Peer reviewed

Evaluating soil nitrate dynamics in an intercropping dripped ecosystem using HYDRUS-2D

Ning Chen [a], Xianyue Li [a,*], Jiří Šimůnek [b], Haibin Shi [a], Qi Hu [a], Yuehong Zhang [a]

[a] College of Water Conservancy and Civil Engineering, Inner Mongolia Agricultural University, Huhhot 010018, China
[b] Department of Environmental Sciences, University of California Riverside, Riverside, CA 92521, USA

HIGHLIGHTS

- N balances in the root zones of intercropped corn and tomatoes were evaluated.
- Soil NO 3-N concentrations in 0–40 cm were higher in tomato region than corn.
- NO_3-N exchange between the bare-corn regions was lower than the bare-tomato.
- HYDRUS-2D modified was calibrated and validated using experimental data.

GRAPHICAL ABSTRACT
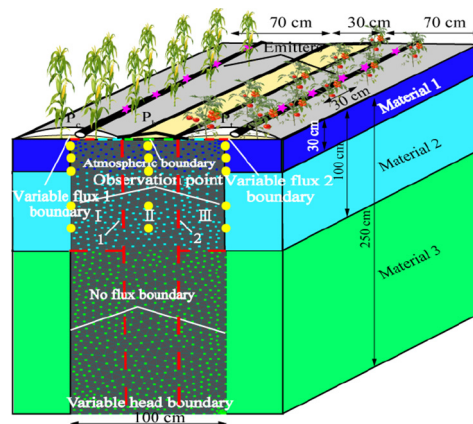
ARTICLE INFO

ABSTRACT

The competition mechanisms between crop species for water and nutrients, especially nitrate (NO_3-N), in intercropping ecosystems are still poorly understood. Therefore, an experiment involving high (300 kg ha^{-1} for corn and 250 kg ha^{-1} for tomato), medium (210 kg ha^{-1} for corn and 175 kg ha^{-1} for tomato), and low (150 kg ha^{-1} for corn and 125 kg ha^{-1} for tomato) N-fertilizer applications (HF, MF, LF, respectively) was conducted in the corn and tomato intercropping ecosystem during 2014 (a calibration period for modeling) and 2015 (a validation period for modeling). The modified HYDRUS-2D code was used to analyze soil NO_3-N concentrations (SNC) in the middle between corn rows (P_c), between corn and tomato rows (P_b), and between tomato rows (P_t), NO_3-N exchange in the horizontal direction between different regions, NO_3-N leaching from the corn, the bare, and the tomato region, and N uptake by crops. Simulated SNCs were in good agreement with measurements, with *RMSE*, *NSE*, and *MRE* of 0.01–0.06 mg cm^{-3}, 0.75–0.98, and 8.7–19.1%, respectively, during the validation period (2015). Average SNCs in the 0–40 cm soil layer were different between P_c, P_t, and P_b. Intensive NO_3-N exchange in the horizontal direction occurred during the second stage (Day After Sowing [DAS] 37-113 in 2014; DAS 29-120 in 2015). NO_3-N exchange between the corn and bare regions was lower than between the tomato and bare regions due to smaller concentration gradients. However, in the vertical direction, NO_3-N leaching from the corn region in both years was 4.1 and 8.8 times larger, respectively, than from the tomato

* Corresponding author.
E-mail address: lixianyue80@126.com (X. Li).

region under HF since NO_3-N mainly moved from the tomato region to the corn region. Our results reveal the competition between corn and tomato for N and provide a rationale for formulating and optimizing different fertilizer regimes for different crops in the intercropping ecosystem.

1. Introduction

Water and fertilizer uptake capacities of multiple crops in an intercropping ecosystem can be very different because of complex agronomic practices and different crop properties. If these differences were optimally managed, the intercropping ecosystem could not only improve the land equivalent ratio (LER) (Martin et al., 2018; Iqbal et al., 2019), water-fertilizer utilization efficiency (Singh et al., 2017; Chen et al., 2019; Du et al., 2019), and light utilization efficiency (LUE), it could also increase crop yields (Hauggaard et al., 2016; Raza et al., 2019; Streit et al., 2019). The intercropping planting pattern can not only increase farmers' income but also has many additional advantages. Therefore, intercropping ecosystems have been extensively used worldwide, including in Germany (Streit et al., 2019), Brazil (Batista et al., 2019), India (Das et al., 2019), Pakistan (Iqbal et al., 2019), and China (Zhou et al., 2019).

Usually, soil water and nitrogen distributions in intercropping ecosystems are different than in single-crop fields because of different resource acquisition strategies, growth, and root distributions of various crop species (Scalise et al., 2017; Chen et al., 2019; Zhao et al., 2019). For example, the results of an experiment in a corn/soybean intercropping ecosystem under full irrigation indicated that the corn roots not only penetrated deeper than those of soybean but also extended into the soybean part of the field to absorb more resources (Gao et al., 2010). Similarly, there were significant differences in the crop root systems in the tomato/corn intercropping ecosystem during the growing season, while the crop root systems of the two species overlapped and competed for soil water and nitrogen (Li et al., 2017).

Root distributions of different crops could cause variations in soil water distributions in the horizontal direction. For example, although irrigation volumes (with the same irrigation frequency) for tomatoes were lower than for corn, the soil water content (SWC) in the shallow root zone (0–40 cm) of tomatoes was higher than in the corn region, especially in the 0–20 cm soil layer (Li et al., 2015). Similarly, SWCs in the alfalfa region were lower than in the corn region in the alfalfa/corn intercropping field under identical irrigation regimes, which caused a low water stress of alfalfa, and the water stress increased as corn grew (Sun et al., 2018).

The movement of nitrogen is closely related to soil water flow, and the difference in SWCs in an intercropping ecosystem could also cause variations in nitrogen distributions, further increasing an intensive nitrogen competition between the crop species. For example, in the corn/pea intercropping and sole crop ecosystems, intercropped pea accumulated more N than sole pea during the crop maturity period, while the opposite occurred for corn (Zhao et al., 2019). Hu et al. (2016) further found that the N competition capacity of pea was 1.35 times larger than of corn. These examples indicate that the N competition capacity of pea is stronger than of corn in the corn/pea intercropping ecosystem. Yang et al. (2016) investigated the long-term effects of an intercropping agroforestry ecosystem (jujube trees with winter wheat/summer corn) on the soil fertility balance. Their results showed that the intercropping ecosystem significantly decreased soil nutrient contents and crop yields, but increased nutrients on the edge of the tree canopy.

In general, optimal nitrogen applications are essential for improving the nitrogen use efficiency (NUE) in the field (Wang et al., 2018; Raza et al., 2019a, 2019b; Noulas et al., 2018). For example, Hartmann et al. (2015) found that a higher recovery efficiency (the components of NUE) could be achieved when the N supply was reduced by 100 kg ha^{-1} from the standard farmers' practice without reducing the crop yield of summer-corn or winter-wheat, while reducing the residual soil mineral N. Nitrate distributions and NUE in intercropping ecosystems were reported in several previous studies (e.g., Ding et al., 2014; Sun et al., 2018; Zhao et al., 2019). However, these studies provided little insight in the water-nitrogen competition between different crop species and were usually carried out under surface irrigation that did not account for various needs of two species in an intercropping ecosystem, causing excessive nitrogen leaching and decreasing NUE, especially for nitrate (Liu et al., 2019). Moreover, these studies did not properly quantify nitrogen fluxes, and due to high time and labor costs, they did not provide a sufficiently long time series of data to evaluate N and water mass balances. Numerical simulations with a calibrated model can overcome these problems and can better reveal soil water and nitrate dynamics.

The HYDRUS-2D model (Šimůnek et al., 2016) has been widely used in the literature to simulate the movement of soil water (Simone et al., 2019, Fan et al., 2018, Filipović et al., 2014, Grecco et al., 2019, Rai et al., 2019, Karandish and Šimůnek, 2018), nitrogen species (He et al., 2018; Grecco et al., 2019; Elasbah et al., 2019), soil salts (Xu et al., 2019), and heat (Rai et al., 2019; Ren et al., 2018). This model can capture the dynamic nature of these factors and be used to optimize their spatial and temporal distributions (Cichota et al., 2018). Additionally, HYDRUS-2D is flexible to accommodate different types of boundary conditions and it is thus widely used to simulate complex conditions. For instance, Wang et al. (2011) estimated subsurface lateral flow and associated NO_3-N losses by modeling the water and nitrogen budgets using HYDRUS-2D in the citrus tree/peanut intercropping ecosystem. On the other hand, Li et al. (2015a, 2015b) used HYDRUS-2D to investigate soil water dynamics in the root zone of the tomato/corn intercropping ecosystem.

Although Li et al. (2015a, 2015b) set independent boundary conditions for each crop, only one set of root water uptake parameters (for the stress response function) could be used in version 2.0 of HYDRUS-2D for two crops, without distinguishing between different water and nitrogen uptake capacities of different crops in an intercropping ecosystem. Therefore, the modified version of HYDRUS-2D, allowing input of two sets of parameters for two vegetations, was used in this study. This modified version can describe the competition between different crops in an intercropping ecosystem for water and nutrient resources.

While earlier studies mainly focused on water or NO_3-N dynamics, there were no studies evaluating exchange processes of soil NO_3-N in the horizontal direction between different crop regions (i.e., the amount of NO_3-N moved from one region to another region). The exchange process of soil NO_3-N in the horizontal direction is an important process, which can reveal the competition for resources by different crops and provide a rationale for formulating and optimizing different fertilizer regimes. Therefore, it is still necessary to quantitatively assess the NO_3-N competition between different crops in an intercropping ecosystem to optimize fertilization.

The main objectives of this study thus are (i) to collect soil water and NO_3-N concentration data and (ii) to calibrate and validate the modified version of HYDRUS-2D that considers two different crops to evaluate these data and simulate soil water and NO_3-N dynamics. Additional objectives are (iii) to assess the temporal and spatial soil NO_3-N distributions, (iv) to analyze the exchange of soil NO3-N in the horizontal direction, and (v) to asses differences in N balances in root zones of corn and tomatoes in an intercropping ecosystem.

Table 1
Agricultural activities during the growing seasons of 2014 and 2015.

Number	Date	Agricultural activities	Remarks
1	April 21 in 2014 and April 25 in 2015	Corn sowing and the base fertilizer application	Before sowing, 300–450 kg ha^{-1} of Diammonium phosphate ($(NH_4)_2HPO_4$, $N \geq 18\%$), and 150 kg ha^{-1} of Potassium sulfate (k_2SO_4) were applied in the field as basal fertilizer.
2	May 10 in 2014 and May 6 in 2015	Tomato transplanting	Laboratory-reared before transplanting
3	May 18 and 27 in 2014 and May 19 in 2015	Irrigation	Irrigations of corn and tomato are 30 and 22.5 mm, respectively.
4	June 4 in 2014 and June 11 in 2015	Irrigation and the N-fertilizer application	Irrigations of corn and tomato are 30 and 22.5 mm, respectively; 30% of the total N-fertilizer
5	June 18 in 2014 and June 26 in 2015	Irrigation	Irrigations of corn and tomato are 30 and 22.5 mm, respectively.
6	July 8 in 2014 and July 4 in 2015	Irrigation and the N-fertilizer application	Irrigations of corn and tomato are 30 and 22.5 mm, respectively; 40% of the total N-fertilizer
7	July 23 and 30 in 2014 and July 19 and 27 in 2015	Irrigation	Irrigations of corn and tomato are 30 and 22.5 mm, respectively.
8	August 10 in 2014 and August 15 in 2015	Irrigation and the N-fertilizer application	Irrigations of corn and tomato are 30 and 22.5 mm, respectively; 30% of the total N-fertilizer
9	August 25 in 2014 and August 20 in 2015	Irrigation of the corn filed	Irrigation is 30 mm
10	September 10 in 2014 and September 6 in 2015	Tomato harvesting	
11	September 26 in 2014 and September 23 in 2015	Corn harvesting	

Note: Events 3 and 7 have more than one day.

2. Material and methods

2.1. Study site, climate and soil description

The study was conducted at the Baleng Saving Water experimental site (40°20′15″N，107°02′05″E) in the Hetao irrigation district, Inner Mongolia, China, over two cropping seasons (from 2014 to 2015). This area, i.e., the Baleng Saving Water experimental site, is characterized by a typical arid climate with mean annual sunlight of 3180 h, mean annual rainfall of 201 mm (very arid conditions), mean annual potential evaporation of 2259 mm (based on 30 years), and mean annual air temperature of 7.7 °C. The soil in the experimental area was classified as silt loam with the following characteristics in the 0–100 cm soil layer: the bulk density of 1.52 g cm^{-3}, the average field capacity (θ_{fc}) of 0.34 cm^3 cm^{-3} (the

volumetric water content). Additionally, the soil in the tillage layer (0–20 cm) was homogeneous, with total nitrogen of 3.00 g kg^{-1}, an organic matter of 56.11 g kg^{-1}, available nitrogen of 1.42 mg kg^{-1}, potassium of 76.90 mg kg^{-1}, and phosphorus of 7.07 mg kg^{-1}.

2.2. Experimental design and treatments

The corn seeds (*Z. mays* L. cv. Zhongdi 77) were sown at the end of April, and the tomatoes (*Solanum lycopersicum.* cv. Dunhe 48) were transplanted into the intercropping field after cultivation in a greenhouse at the beginning of May in the 2014 and 2015 seasons. The harvest dates were September 26 and 23 for corn in 2014 and 2015, respectively, and September 10 and 6 for tomato, respectively (Table 1). The planting pattern was "one film mulch, one drip line,
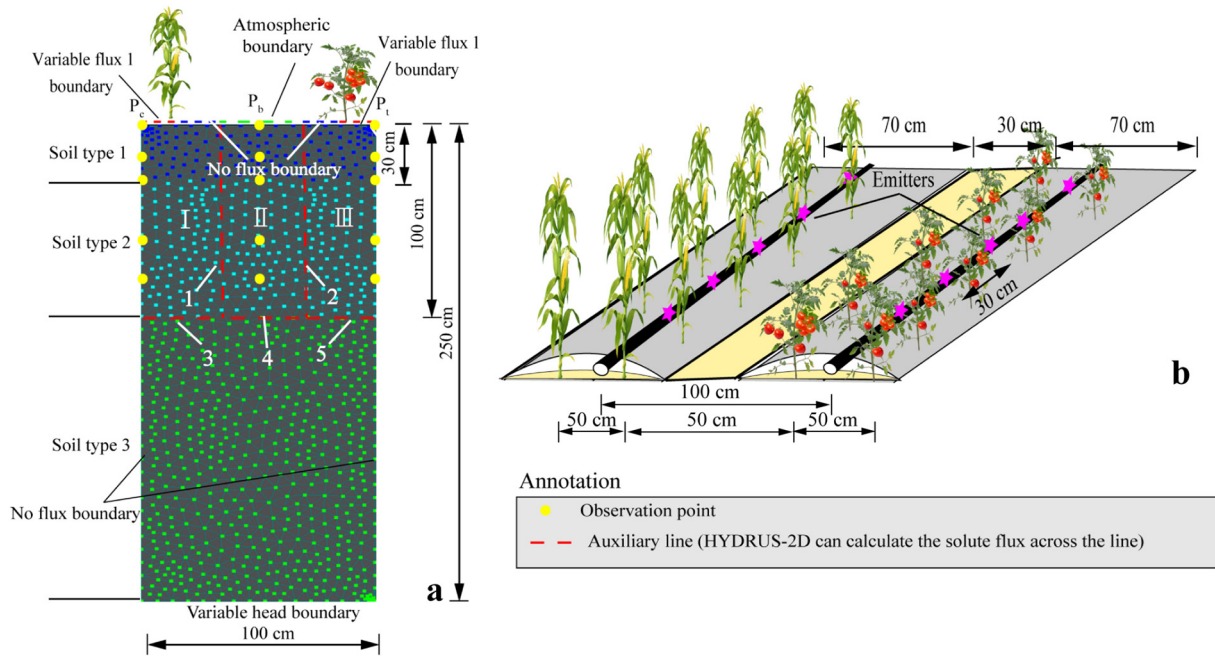
Fig. 1. The modeling domain, boundary conditions (a), and planting pattern (b) for the corn/tomato intercropping ecosystem. Numbers I, II, and III refer to the corn, bare, and tomato regions, respectively. Lines 1 and 2 are between regions I and II, and II and III, respectively. Lines 3, 4, and 5 are located at a depth of 100 cm below the corn, bare, and tomato regions, respectively. Points P_c, P_b, and P_t are located in the middle between corn rows, between corn and tomato rows, and between tomato rows, respectively.

two crop lines," and two rows of tomatoes were sown between corn rows (Fig. 1). The seed rate was 11,000 viable seeds ha^{-1} for corn, and the real number of transplanted tomato plants was 408 for each plot.

Before sowing, 300 kg ha^{-1} of Diammonium phosphate ((NH$_4$)$_2$HPO$_4$, $N \geq 18\%$), and 150 kg ha^{-1} of Potassium sulfate (K$_2$SO$_4$) were applied by broadcast fertilization in the field as basal fertilizer. The experimental design was a completely random design comprising of three replicates of three topdressing treatments, i.e., 9 field plots. Every plot was 9.2 m wide and 15 m long. The high N-fertilizer application of 300 kg ha^{-1} for corn (HF$_c$) and 250 kg ha^{-1} for tomato (HF$_t$) was based on local recommendations. Additionally, different levels of N-fertilizer, i.e., 70% and 50% of recommended N-fertilizer, were applied in the corn and tomato fields. There were thus three levels of applied topdressing N-fertilizer: HF$_c$ and HF$_t$ (the local recommendation), MF$_c$ and MF$_t$ (70% of the local recommendation), and LF$_c$ and LF$_t$ (50% of the local recommendation). The Carbamide solution (CO(NH$_2$)$_2$, $N \geq 32\%$) as topdressing was applied in the field in the elongation stage (30% of the total N-fertilizer), the tasseling stage (40% of the total N-fertilizer), and the filling stage (30% of the total N-fertilizer), each time accompanied with drip irrigation with an emitter discharge of 2.4 L h^{-1} and a distance of 30 cm. The water meter (with an accuracy of 0.001 L) was set up to monitor water flow. The groundwater table at the experimental site was monitored using the auto water level logger (Onset Computer Inc.; U20L-01, Hobo, USA) and was 83–248 cm deep in 2014 and 2015. Large variations in the depth of the groundwater table were caused by a nearby irrigation canal. A list of performed agricultural activities is summarized in Table 1.

2.3. Measurements and methods

Meteorological data, i.e., daily precipitation, solar radiation, air temperatures, air humidity, and wind speed, were collected in the experimental field using the automatic meteorological station (Onset Computer Inc.; U30, Hobo, USA) at 30 s intervals, and the 10-min statistics (average) were computed. Reference crop evapotranspiration (ET_0) was then calculated using the Penman-Monteith approach (Allen et al., 1998). Daily evapotranspiration (ET_c) rates for different crop stages were calculated by multiplying ET_0 by K_c (the crop coefficient) that were taken from the FAO paper (No.56). A list of specific dates of the different crop stages for corn and tomato is summarized in Table 2.

The initial soil water contents (SWCs) were measured using gravimetric measurements before sowing. TDR probes (IMKO GmbH Inc.; IPH, TRIME-PICO, Germany) were installed in the middle between corn rows (P$_c$), between corn and tomato rows (P$_b$), and between tomato rows (P$_t$) (Fig. 1) for measuring SWCs during the crop growing season. SWCs were taken once every 7 days at soil depths of 0–20, 20–40, and 40–100 cm, and the data were verified by gravimetric measurements at periodic intervals (Skaggs et al., 2004).

Soil samplings for nitrate (NO$_3$-N) concentrations were taken at the same locations as SWCs every two weeks. Soil samples were shaken with 2 mol L^{-1} KCl (1:5 soil:solution ratio) for 1 h, and the obtained extract was analyzed using a spectrophotometer (Beijing General Instrument Co. LTD., TU-1901, General Instrument, CHN). Total N uptake was determined on the same dates using ten plants randomly harvested from each plot to determine total N uptake by the crop stem, leaves, and grains. These samples were first kept for 30 min at 105 °C temperature

and then conserved at 75 °C temperature in the oven to reach a constant weight. After crushing and sifting, a 0.2 g sample was weighted by a weighing paper, boiled with 5 mL of concentrated H$_2$SO$_4$, and then measured by a flow analyzer (Brown ruby Inc., AA3, SEAL, Germany). The ultraviolet spectrophotometry method (GB/T 32737-2016) and the semi-micro Kjeldahl method (Bremner and Keeney, 1965) were applied to determine NO$_3$-N concentrations in soil (SNC) and total N in crops (N_c) using the following formulas:

$$SNC = \frac{\rho \times V \times D \times \gamma_s}{m} \tag{1}$$

where SNC is the NO$_3$-N concentration (mg cm^{-3}), ρ is the mass concentration of NO$_3$-N in the chromogenic solution (mg mL^{-1}), V is the volume of the chromogenic solution (mL), D is the dilution ratio (-), m is the soil mass (g), and γ_s is the dry bulk density (g cm^{-3}).

$$N_c = \frac{C \times V \times V_T \times 14}{V_s} \times 6.25 \times 1000 \tag{2}$$

In Eq. (2), N_c is the total N concentration in the crop stem, leaves, and grains (mg kg^{-1}), C is the mass concentration of HCl in the titrant (mg mL^{-1}), V is the volume of the titrant (mL), V_T is the total volume of the solution (mL), and V$_s$ is the volume of the measured solution (mL).

$$NU = m_c \cdot N_c \tag{3}$$

In Eq. (3), NU is N uptake (mg), and m_c is the dry mass of the crop (kg).

The leaf area meter (Li-3000, LI-COR, USA) and a tape (with the accuracy of 0.1 cm) were used to measure the leaf area and crop height, respectively, for corn and tomatoes with three replicates once every 7–15 days and the leaf area index (LAI) was calculated using the FAO method (Allen et al., 1998).

Root samples for corn and tomatoes under good growth conditions were collected from a soil transect using a method of Li et al. (2017) during the elongation stage (June 12 and 8 in 2014 and 2015, respectively), the tasseling stage (June 25 and 18 in 2014 and 2015, respectively), the filling stage (July 11 and 18 in 2014 and 2015, respectively), and the maturation stage (August 20 and 23 in 2014 and 2015, respectively). These samples were collected every 5 cm down to a depth of 50 cm where higher roots density occurred, and then every 10 cm below the 50-cm depth until no roots were found. The root samples were first washed and solarized, and then scanned using the Epson Perfection V700 PHOTO. The roots parameters (the root length, root surface area, and root volume) were determined using the WinRHIZO software.

2.4. Modeling description

2.4.1. Modeling introduction

The HYDRUS-2D model modified to consider simultaneously two vegetations was used to simulate the transient two-dimensional movement of water and solutes in the soil profile. This program numerically solves the Richards equation for variably-saturated water flow and advection-dispersion equations for solute transport. The model additionally allows the specification of different root water and solute uptake parameters for different crops, which affects the spatial distribution of water and nitrate between irrigation cycles. The solute equation considers the advective-dispersive transport in the liquid phase, as well as diffusion in the gaseous phase. The theoretical part of the model is described in detail in the technical manual (Šimůnek et al., 2016).

2.4.2. Soil hydraulic properties

The soil hydraulic parameters for the van Genuchten-Mualem model for different soil layers (0–30, 30–100, and 100–250 cm) were

Table 2
The dates of different crop stages for corn and tomato used to compute ET_p during 2014 and 2015.

Crop	Year	Early season	Mid-season	Late season
Corn	2014	April 21–May 27	May 28–August 12	August 13–September 26
	2015	April 25–May 23	May 24–August 23	August 24–September 23
Tomato	2014	May 10–June 1	June 2–August 15	August 16–September 10
	2015	May 6–June 5	June 6–August 18	August 19–September 6

Table 3
Soil textural properties and soil hydraulic parameters for the 0–250 cm soil layer.

Soil layer (cm)	Soil particle size distribution (%)			Residual soil water content θ_r ($cm^3 \cdot cm^{-3}$)	Saturated soil water content θ_s ($cm^3 \cdot cm^{-3}$)	Shape parameter α (cm^{-1})	Shape parameter n (−)	Saturated hydraulic conductivity K_s ($cm \cdot day^{-1}$)
	Clay	Silt	Sand					
0–30	4.8	39.0	56.2	0.03	0.41	0.02	1.45	55.4
30–100	3.0	56.1	40.9	0.04	0.42	0.01	1.63	52.0
100–250	8.3	59.2	32.5	0.05	0.41	0.01	1.63	37.9

estimated using the Rosetta software package (Schaap et al., 2001) in HYDRUS-2D. Initial estimates of soil hydraulic parameters were based on soil textural information (% of sand, silt, and clay) and the bulk density. Additionally, these values of soil hydraulic parameters (e.g., shape parameters and the saturated hydraulic conductivity) for three soil layers were further manually calibrated by comparing simulated and observed values of SWCs and SNCs. Calibrated values of soil hydraulic parameters are shown in Table 3.

2.4.3. Root water uptake parameters for corn and tomato

HYDRUS-2D was modified to consider water and N uptake by roots of two vegetations, i.e., to allow different parameters for root water uptake by corn and tomatoes. Root water extraction was computed according to the Feddes model (Feddes et al., 1978; Šimůnek and Hopmans, 2009) adapted for two-dimensional conditions with two crops:

$$S(h) = [\alpha_1(h) \cdot b_1(x,z) + \alpha_2(h) \cdot b_2(x,z)] \cdot T_p \cdot S_t \qquad (4)$$

where T_p is the potential transpiration rate (cm day^{-1}), S_t is the surface length associated with transpiration (cm), $b_1(x,z)$ and $b_2(x,z)$ are root water uptake distribution functions (cm^{-2}) for corn and tomatoes, respectively, which can be calculated based on measured root distributions (Fig. 2), and $a_1(h)$ and $a_2(h)$ are root water uptake stress reduction functions for corn and tomatoes, respectively, which can be

calculated as follows:

$$\alpha(h) = \begin{cases} \dfrac{h_1-h}{h_1-h_2} & h_2 < h \leq h_1 \\ 1 & h_3 \leq h \leq h_2 \\ \dfrac{h-h_4}{h_3-h_4} & h_4 \leq h < h_3 \end{cases} \qquad (5)$$

where h_1 is the anaerobic point pressure head (cm), h_2 and h_3 are optimal interval pressure heads (cm), h_4 is the wilting point pressure head (cm); specific parameters are listed in Table 4 (Wesseling and Brandyk, 1985).

2.4.4. Solute parameters

Solute reaction processes include nitrification, denitrification, volatilization, immobilization, and mineralization. In this study, the denitrification process and the losses in the form of N$_2$O-N can be neglected because this reaction occurs mainly under saturated conditions (Ravikumar et al., 2011). The processes of immobilization and mineralization were also neglected, similarly as in many other modeling studies (Ravikumar et al., 2011; Ramos et al., 2012; Tafteh and Sepaskhah, 2012), due to the low clay content in the experimental soil, which is often correlated with these two processes. Ammonia volatilization was neglected due to the fertilizer application with irrigation water (Ramos et al., 2012). The applied fertilizer was ammonium nitrate, which transforms first into NO$_2$-N, and then further into NO$_3$-N. Since, the nitrification process from NO$_2$-N to NO$_3$-N is much faster than
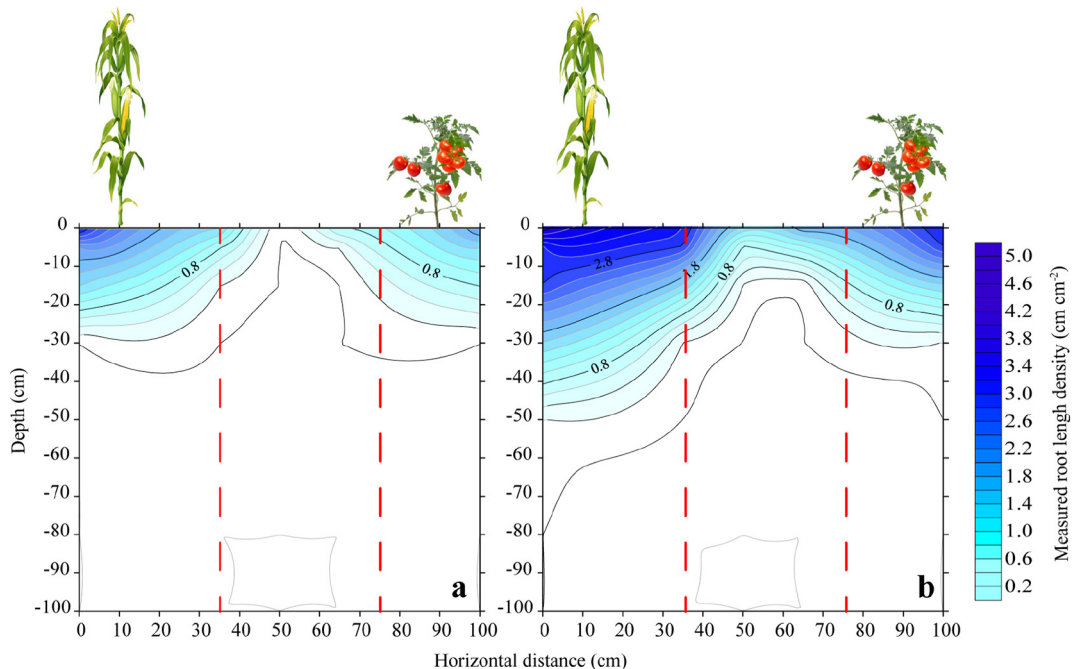
Fig. 2. Measured average distributions of corn and tomato roots during May–July (a) and July–September (b) in 2014 and 2015.

Table 4
Parameters of the stress response function for root water uptake by corn and tomato.

Crop	h_1 (cm)	h_2 (cm)	h_3 (cm)	h_4 (cm)
Corn	−15	−325	−600	−8000
Tomato	−30	−800	−1500	−8000

from NH_4-N to NO_2-N, the nitrification process can be assumed to proceed directly from NH_4-N into NO_3-N, which is consistent with many other studies (Wang et al., 2010; Tafteh and Sepaskhah, 2012). The nitrification process in HYDRUS-2D is simulated as a first-order decay reaction. The nitrification rates for reactions in the liquid and solid phases were set to 0.12 and 5.9 d^{-1}, respectively (Castaldelli et al., 2018). The temperature and water content dependencies of the nitrification process were not considered, similarly as in many other modeling studies (Ravikumar et al., 2011; Ramos et al., 2012; Tafteh and Sepaskhah, 2012; Li et al., 2015a, 2015b). This study also assumed that NO_3-N is present only in the dissolved phase, while ammonium is also adsorbed to the solid phase. The distribution coefficients (K_d) were thus set to 0 and 3.5 cm^3 g^{-1} for NO_3-N and NH_4-N, respectively (Hanson et al., 2006).

Soil longitudinal and transversal dispersivities (D_L and D_T, respectively) and the molecular diffusion coefficient in free water are needed to determine the components of the dispersion tensor. Longitudinal dispersivities (D_L) were considered to be 10, 10, and 5 cm for the 0–30, 30–100, and 100–250 cm soil layers, respectively; these values were obtained using the trial-and-error calibration method, i.e., by comparing simulated and observed values of soil NO_3-N concentrations. The transverse dispersivity (D_T) was taken as one-tenth of D_L (Hanson et al., 2006; Ramos et al., 2012). Molecular dispersivity coefficients of NH_4-N and NO_3-N in free water were set to be 0.064 and 0.068 cm2 h^{-1}, respectively (Cote et al., 2003).

2.4.5. Initial and boundary conditions

The two-dimensional transport domain was defined as a rectangle with a width of 100 cm and a depth of 250 cm (Fig. 1). Observed values of SWCs were used as the initial condition in the model. Due to the coarse soil texture and the low initial fertilizer content, the initial conditions for NH_4-N and NO_3-N concentrations were defined to be zero. Besides, horizontal distributions of initial SWCs and NO_3-N concentrations were assumed to be uniform.

Four boundaries were defined in HYDRUS-2D, i.e., the upper boundary, the bottom boundary, and two lateral boundaries (the left and right boundary). The time-variable flux and atmospheric boundary conditions were specified at the two emitters (in corn and tomato rows) and the soil surface, respectively, to represent drip irrigation and to apply precipitation, potential evaporation, and transpiration fluxes, respectively. Potential evaporation (E_p) and transpiration (T_p) can be obtained as fractions of potential evapotranspiration (ET_p) (Campbell and Norman, 1989), while ET_p can be obtained by multiplying ET_0 with the crop coefficient (K_c) as follows:

$$ET_{p1} = ET_0 \cdot K_{c1} \tag{6}$$
$$ET_{p2} = ET_0 \cdot K_{c2} \tag{7}$$

Table 5
RMSE, NSE, and MRE for measured and simulated SWCs and SNCs under high (HF), medium (MF), and low (LF) N-fertilizer applications in regions between corn rows (P_c), between corn and tomato rows (P_b), and between tomato rows (P_t) during calibration (2014) and validation (2015).

Year	Treatments		Depth (cm)	Crop regions						Bare area		
				P_c			P_t			P_b		
				RMSE	NSE	MRE	RMSE	NSE	MRE	RMSE	NSE	MRE
2014	SWCs	HF	0–20	0.03	0.85	11.0%	0.03	0.95	10.0%	0.02	0.93	10.2%
			20–40	0.02	0.92	7.6%	0.02	0.96	7.3%	0.02	0.95	8.6%
			40–100	0.03	0.90	8.1%	0.02	0.99	7.2%	0.03	0.96	8.8%
		MF	0–20	0.04	0.83	12.1%	0.04	0.85	12.0%	0.02	0.95	9.8%
			20–40	0.03	0.84	10.0%	0.03	0.93	9.1%	0.04	0.92	10.5%
			40–100	0.03	0.90	9.6%	0.03	0.98	7.5%	0.03	0.88	10.8%
		LF	0–20	0.04	0.87	11.2%	0.04	0.85	11.5%	0.04	0.81	13.5%
			20–40	0.03	0.88	10.5%	0.02	0.92	10.3%	0.03	0.90	10.6%
			40–100	0.03	0.93	9.8%	0.03	0.95	8.7%	0.03	0.91	9.8%
		HF	0–20	0.03	0.83	11.2%	0.04	0.82	10.4%	0.05	0.85	12.7%
	SNCs		20–40	0.01	0.99	9.9%	0.02	0.97	9.9%	0.03	0.93	10.6%
			40–100	0.02	0.89	8.6%	0.02	0.87	8.5%	0.02	0.88	9.3%
		MF	0–20	0.02	0.85	12.9%	0.03	0.88	11.7%	0.03	0.81	19.5%
			20–40	0.02	0.86	15.8%	0.04	0.83	15.4%	0.04	0.82	18.9%
			40–100	0.01	0.95	11.5%	0.04	0.87	13.1%	0.01	0.84	16.9%
		LF	0–20	0.03	0.92	10.1%	0.05	0.82	12.7%	0.05	0.80	16.7%
			20–40	0.04	0.87	13.1%	0.04	0.84	10.5%	0.04	0.84	14.8%
			40–100	0.02	0.97	10.5%	0.03	0.89	9.1%	0.02	0.91	12.2%
2015	SWCs	HF	0–20	0.03	0.82	11.7%	0.03	0.89	10.6%	0.04	0.83	12.5%
			20–40	0.02	0.90	9.2%	0.02	0.96	9.7%	0.02	0.86	9.1%
			40–100	0.03	0.90	8.4%	0.03	0.92	10.5%	0.03	0.95	7.9%
		MF	0–20	0.04	0.86	11.5%	0.03	0.89	10.1%	0.02	0.86	12.3%
			20–40	0.05	0.85	12.4%	0.02	0.94	7.6%	0.07	0.82	12.7%
			40–100	0.04	0.91	10.1%	0.03	0.92	9.6%	0.03	0.87	8.7%
		LF	0–20	0.04	0.86	12.8%	0.04	0.90	9.9%	0.05	0.79	14.3%
			20–40	0.02	0.90	9.7%	0.03	0.91	8.1%	0.03	0.84	11.7%
			40–100	0.03	0.88	10.8%	0.03	0.91	9.6%	0.03	0.89	8.8%
		HF	0–20	0.03	0.82	12.0%	0.04	0.95	12.0%	0.04	0.84	13.7%
	SNCs		20–40	0.03	0.90	10.6%	0.03	0.95	9.7%	0.04	0.96	10.7%
			40–100	0.02	0.86	8.7%	0.02	0.96	8.9%	0.02	0.98	9.1%
		MF	0–20	0.03	0.83	13.5%	0.04	0.84	15.7%	0.06	0.75	18.1%
			20–40	0.02	0.92	10.7%	0.02	0.87	12.7%	0.05	0.83	15.1%
			40–100	0.01	0.90	12.2%	0.02	0.91	11.5%	0.02	0.88	13.2%
		LF	0–20	0.03	0.82	14.2%	0.04	0.81	14.5%	0.06	0.83	15.4%
			20–40	0.03	0.85	11.5%	0.03	0.85	11.7%	0.05	0.86	13.7%
			40–100	0.01	0.90	10.2%	0.02	0.83	13.4%	0.03	0.87	11.3%

$$T_{p1} = \{1 - \exp(-k \cdot LAI)\} \cdot ET_{p1} \tag{8}$$

$$T_{p2} = \{1 - \exp(-k \cdot LAI)\} \cdot ET_{p2} \tag{9}$$

$$E_{p1} = ET_{p1} - T_{p1} \tag{10}$$

$$E_{p2} = ET_{p2} - T_{p2} \tag{11}$$

where ET_{p1} and ET_{p2} are the potential evapotranspiration rates in the corn and tomato regions (cm day^{-1}), respectively, T_{p1} and T_{p2} are the potential transpiration rates in the corn and tomato regions (cm day^{-1}), respectively, E_{p1} and E_{p2} are the potential evaporation rates in the by corn and tomato regions (cm day^{-1}), respectively, and K_{c1} and K_{c2} are the crop coefficients for corn and tomato, respectively, that were taken from the FAO paper (Allen et al., 1998). K_{c1} is equal to 0.30 during the early season, 1.20 during the mid-season, and 0.35 during the late season; K_{c2} is 0.60 during the early season, 1.15 during the mid-season, and 0.70 during the late season (Allen et al., 1998). The extinction coefficient k is equal to 0.39 for corn (Li et al., 2018) and 0.65 for tomato (Cruz et al., 2014).

The emitter fluxes in the corn and tomato regions were represented in HYDRUS-2D with two 10 cm long time-variable boundary conditions and were calculated as follows:

$$q = Q/L' \tag{12}$$

where q is the boundary flux (cm day^{-1}), Q is the actual emitter flux (cm^2 day^{-1}), and L' is the width of the variable flux boundary condition (cm).

The solute flux across a particular boundary or between two regions, q_c (mg cm^{-2} day^{-1}), can be calculated using the following equation:

$$q_c = q \times SNC \tag{13}$$

where q is the water flux (cm day^{-1}), and SNC is the NO$_3$-N concentration (mg cm^{-3}). The solute exchange (the amount of NO$_3$-N moving between different regions), Q_s (mg cm^{-1}), can be calculated using the following equation:

$$Q_S = q_c \times L \times t \tag{14}$$

where L is the length of the boundary or mesh-line (cm), i.e., the line separating the two regions, and t is the time (day).

A time-variable head boundary condition was applied along the bottom boundary, which considers the effect of the shallow groundwater table on flow and soil nitrate dynamics. Additionally, the third-type Cauchy boundary condition was used for solute transport along all boundaries with specified water fluxes (at the top boundary), while the second-type Neumann boundary condition was used for solute transport along outflow boundaries (at the bottom boundary). Two lateral boundaries of the flow domain were assigned a no-flow boundary condition.

2.5. Statistical analysis

Significant differences in soil water contents and soil NO$_3$-N concentrations were analyzed using the ANOVA method using the SPSS software (SPSS Inc., 20.0., USA). For evaluating the model performance in simulating soil water dynamics and the NO$_3$-N fate and transport under different N-fertilizer applications, the root mean square error (RMSE), the Nash-Sutcliffe (NSE), and the mean relative error (MRE) were computed for observed and simulated values. The specific formulas are as follow:

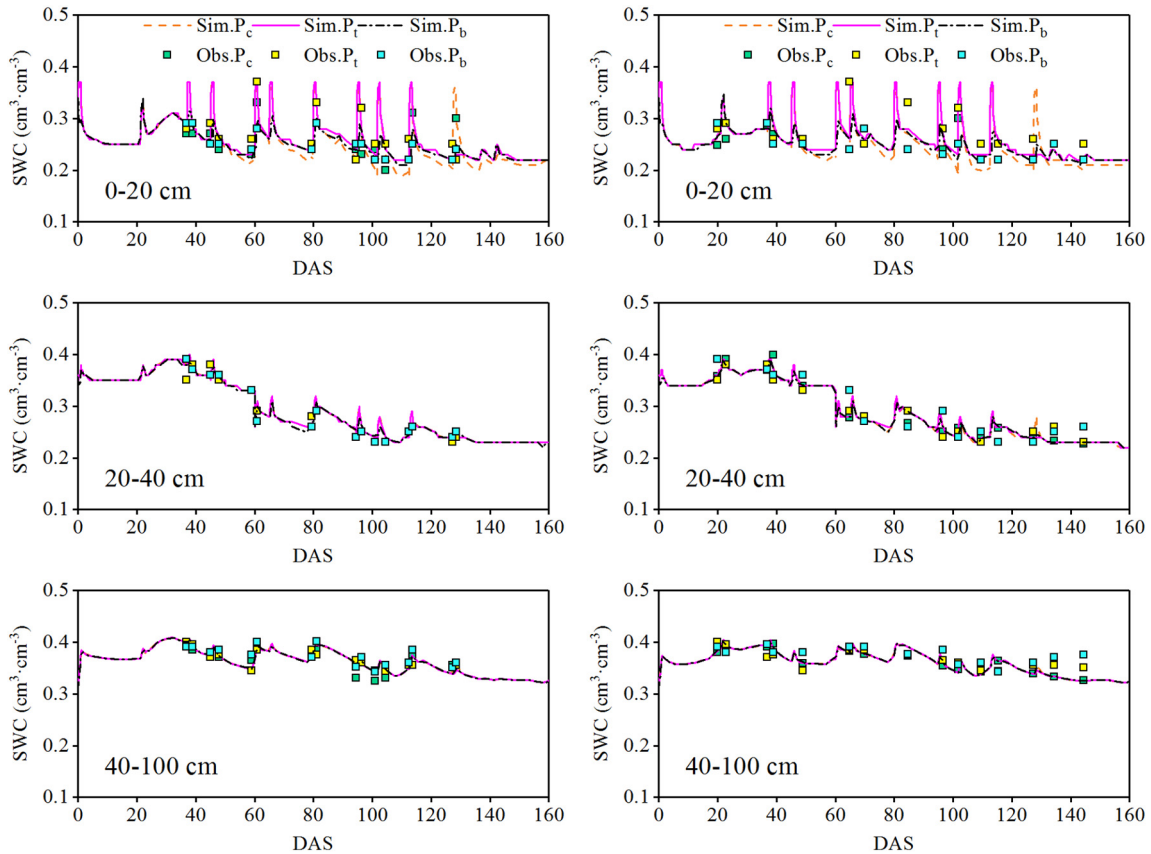$$RMSE = \sqrt{\frac{1}{n}\sum_{i=1}^{n}(S_i - O_i)^2} \tag{15}$$

Fig. 3. Simulated soil water contents (SWCs) in regions between corn rows (P$_c$), between corn and tomato rows (P$_b$), and between tomato rows (P$_t$) in the 0–20 (top), 20–40 (middle), and 40–100 (bottom) cm soil layers in 2014 (left) and 2015 (right) for the high N-fertilizer application (HF).

$$NSE = 1 - \frac{\sum_{i=1}^{n}(S_i - O_i)^{2^n}}{\sum_{i=1}} \ (O_i - \overline{O})^2 \qquad (16)$$

$$MRE = \frac{1}{n}\sum_{i=1}^{n} \frac{|S_i - O_i|}{S_i} \times 100\% \qquad (17)$$

where S_i and $\overline{S}$ are individual and mean simulated soil NO_3-N concentration values (mg cm^{-3}), respectively, O_i and $\overline{O}$ are individual and mean observed soil NO_3-N concentration values (mg cm^{-3}), respectively, and n is the number of observed values.

3. Results

3.1. Soil NO_3-N concentration calibration and verification

Observed values of soil water contents (SWCs) and soil NO_3-N concentrations (SNCs) under different N-fertilizer application levels at different crop locations during 2014 and 2015 were used for model calibration and validation, respectively. Table 5 shows that *RMSE*, *NSE*, and *MRE* for measured and simulated SWCs under different N-fertilizer application levels (HF, MF, LF) during the calibration period (2014) are in the range of 0.02–0.04 cm^3 cm^{-3}, 0.81–0.99, and 7.2–13.5%, respectively, and for SNCs in the range of 0.01–0.05 mg cm^{-3}, 0.80–0.99, and 8.5–18.9%, respectively. During the validation period (2015), they are in similar ranges of 0.02–0.07 cm^{3}cm^{-3}, 0.79–0.96, and 7.6–14.3%, respectively, for SWCs, and 0.01–0.06 mg cm^{-3}, 0.75–0.98 and 8.7–19.1%, respectively, for SNCs. Additionally, visual inspection (Figs. 3 and 4) was used to assess the correspondence between simulated and observed SWCs and SNCs under the high N-fertilizer application (HF). Small statistical errors between simulated and observed SNC values during both calibration and validation periods indicate that HYDRUS-2D can well capture the NO_3-N dynamics even though the processes of volatilization, immobilization, and mineralization have been neglected.

3.2. Soil NO_3-N distribution in the soil profile in an intercropping ecosystem

In order to evaluate the effects of different N-fertilizer application levels on soil NO_3-N distributions in the soil profile (0–100 cm) of the corn/tomato intercropping ecosystem, DAS 80 and 85 in 2014 and DAS 84 and 89 in 2015 were selected (i.e., one day before and five days after the N-fertilizer application).

One day before the N-fertilizer application (DAS 80 in 2014 and DAS 84 in 2015), SNCs in the middle between corn rows (P_c) and tomato rows (P_t) were higher than in the middle between corn and tomato rows (P_b) because film mulching reduced water vapor exchange (soil evaporation) between the surface soil and the atmosphere and promoted the mineralization rate. The average SNCs under the high N-fertilizer application (HF) in the shallow soil layer (0–40 cm) were 32.1 and 47.5% higher in P_c and P_t, respectively than in P_b during 2014 and 2015, 22.8 and 34.2% higher, respectively, under the medium N-fertilizer application (MF), and 16.4 and 24.2% higher, respectively, under the low N-fertilizer application (LF). Additionally, the roots of corn and tomato were mainly distributed in the 0–40 cm soil layer. Since N uptake of corn was considerably higher than that of tomato, the SNC in P_c was lower than in P_t in the shallow soil layer. The average SNCs for HF, MF, and LF were on average in both years (2014 and 2015) reduced by 30.9, 24.8, and 19.8%, respectively, in P_c compared with P_t.

SNCs increased in all treatments after the N-fertilizer application (Fig. 5b, d, f, h, j, and l). There were obvious increases in SNCs in the P_c and P_t regions due to direct fertilizer applications. Moreover, the SNC in P_b increased not only due to the high N-fertilizer application but
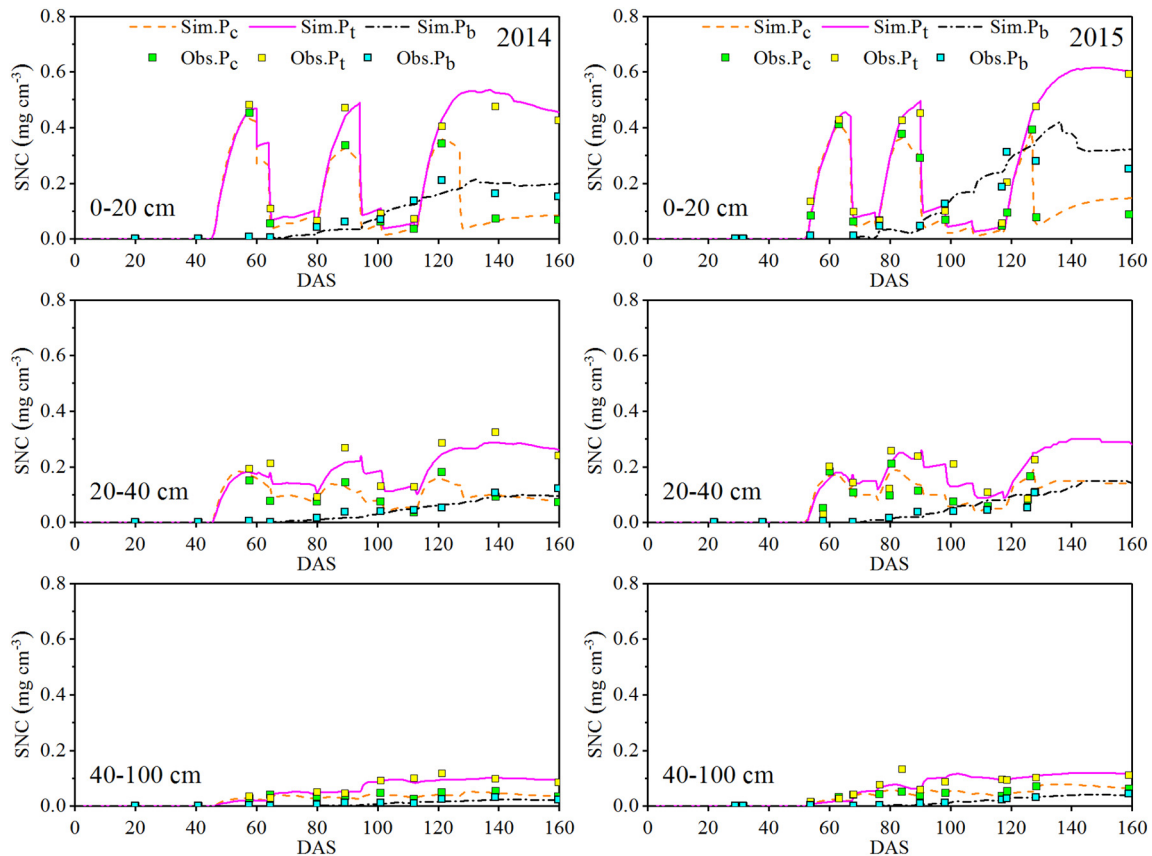

Fig. 4. Simulated soil NO_3-N concentrations (SNCs) in regions between corn rows (P_c), between corn and tomato rows (P_b), and between tomato rows (P_t) in the 0–20 (top), 20–40 (middle), and 40–100 (bottom) cm soil layers in 2014 (left) and 2015 (right) for the high N-fertilizer application (HF).

also due to the flow of NO$_3$-N with irrigation water from the crop regions (P$_c$ and P$_t$) to the bare region (P$_b$). However, there were little variations in the SNC in P$_c$ and P$_t$ in the 40–100 cm soil layer because of a lower irrigation water footprint.

3.3. Soil NO$_3$-N dynamic in the horizontal direction

The modeling domain was divided into three regions for studying NO$_3$-N exchange in the intercropping ecosystem, i.e., the corn region (I), the bare region (II), and the tomato region (III) (Fig. 1). Additionally, the entire crop growing season was divided into three growth stages, similarly to the crop stages for computing ET$_p$ (Table 2): the first stage (DAS 0-36 in 2014 and DAS 0-28 in 2015, i.e., slow NO$_3$-N exchange), the second stage (DAS 37-113 in 2014 and DAS 29-120 in 2015, i.e., intensive NO$_3$-N exchange), and the third stage (DAS 114-158 in 2014 and DAS 121-151 in 2015, i.e., stable NO$_3$-N exchange).

In general, the roots of the two crops may overlap during the late crop growing season, resulting in one crop taking up resources from another crop's root zone. However, since this process was relatively small, the soil NO$_3$-N concentration was not much affected by the overlap of the two root systems. In order to differentiate between the effects of different resource absorption capacities of the two crops on soil NO$_3$-N movement in the intercropping ecosystem, it was assumed in this study that the crop roots grew only in its own root zone, and the two root systems do not overlap. Therefore, the N competition mechanisms of different crops can be found using the analysis of NO$_3$-N exchange between different regions.

During the first stage, there was no intensive NO$_3$-N exchange due to relatively dry soil and small concentration gradients. As crops grew, NO$_3$-N exchange between different root zones increased. During the second stage, NO$_3$-N moved in both year in the horizontal direction from the crop regions (I and III) to the bare region (II) (Fig. 6), and simulated NO$_3$-N exchange was 38.4, 26.9, and 19.2 mg cm^{-1} under HF, MF, and LF, respectively. Simulated outflow of NO$_3$-N from the bare region (II) into the crop regions (I and III) was 4.6, 3.2, and 2.3 mg cm^{-1} under HF, MF, and LF, respectively, and annual net inflows (inflow of NO$_3$-N into minus outflow of NO$_3$-N out of the region) were 33.9, 23.7, and 16.9 mg cm^{-1}, respectively. On the other hand, different N-fertilizer applications and different uptake capacities of corn and tomato caused different NO$_3$-N inflow into the bare region (II) from the corn and tomato regions (I and III, respectively). Average simulated NO$_3$-N exchanges between the corn region (I) and the bare region (II) were 12.5, 8.8, and 6.3 mg cm^{-1} under HF, MF, and LF in both years, respectively, while average simulated NO$_3$-N fluxes were 0.10, 0.07, and 0.05 mg cm^{-2} day^{-1}, respectively. Average simulated NO$_3$-N exchange of 25.9, 18.1, and 13.0 mg cm^{-1} under HF, MF, and LF, respectively, were transferred from the tomato (III) to the bare region (II) in both years, while the average soil NO$_3$-N flux was 0.21, 0.14, and 0.10 mg cm^{-2} day^{-1}. Additionally, the soil NO$_3$-N also moved from the bare region (II) to the crop regions (I and III) during some periods of the N-fertilizer application. For example, average NO$_3$-N exchange between the bare (II) to the corn region (I) were 3.6, 2.5 and 1.8 mg cm^{-1} under HF, MF and LF in both year, respectively, while 1.0, 0.7 and 0.5 mg cm^{-1} of NO$_3$-N were transmitted into the
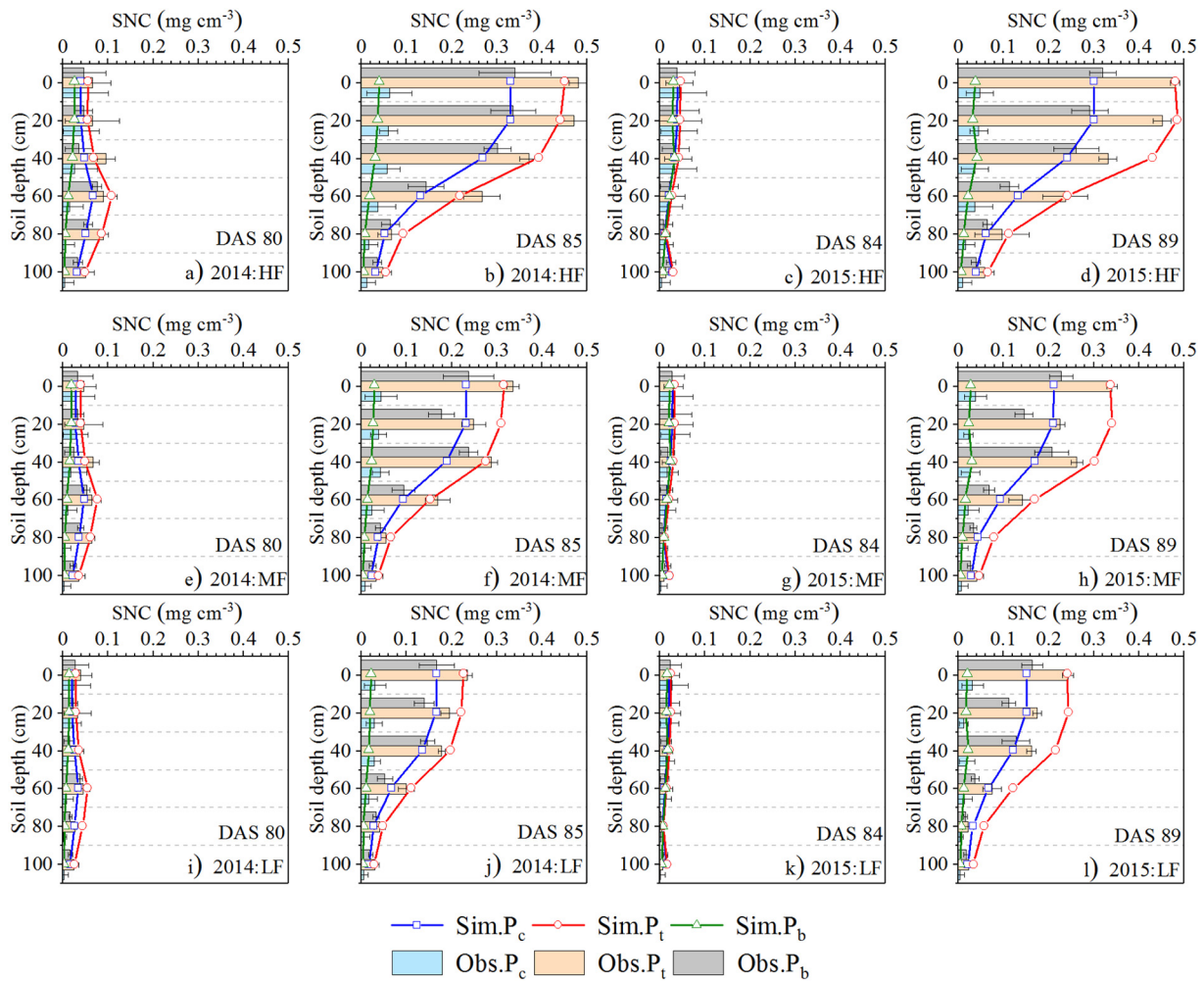

Fig. 5. Simulated soil NO$_3$-N concentrations (SNC) in the region between corn rows (P$_c$), between corn and tomato rows (P$_b$), and between tomato rows (P$_t$) in the soil profile (0–100 cm) one day before (DAS 80 and 84 in 2014 and 2015, respectively) and five days after (DAS 85 and 89 in 2014 and 2015, respectively) the N-fertilization application for the high (HF), medium (MF), and low (LF) N-fertilizer application. (a, b, e, f, i, and j for 2014; c, d, g, h, k, and l for 2015).
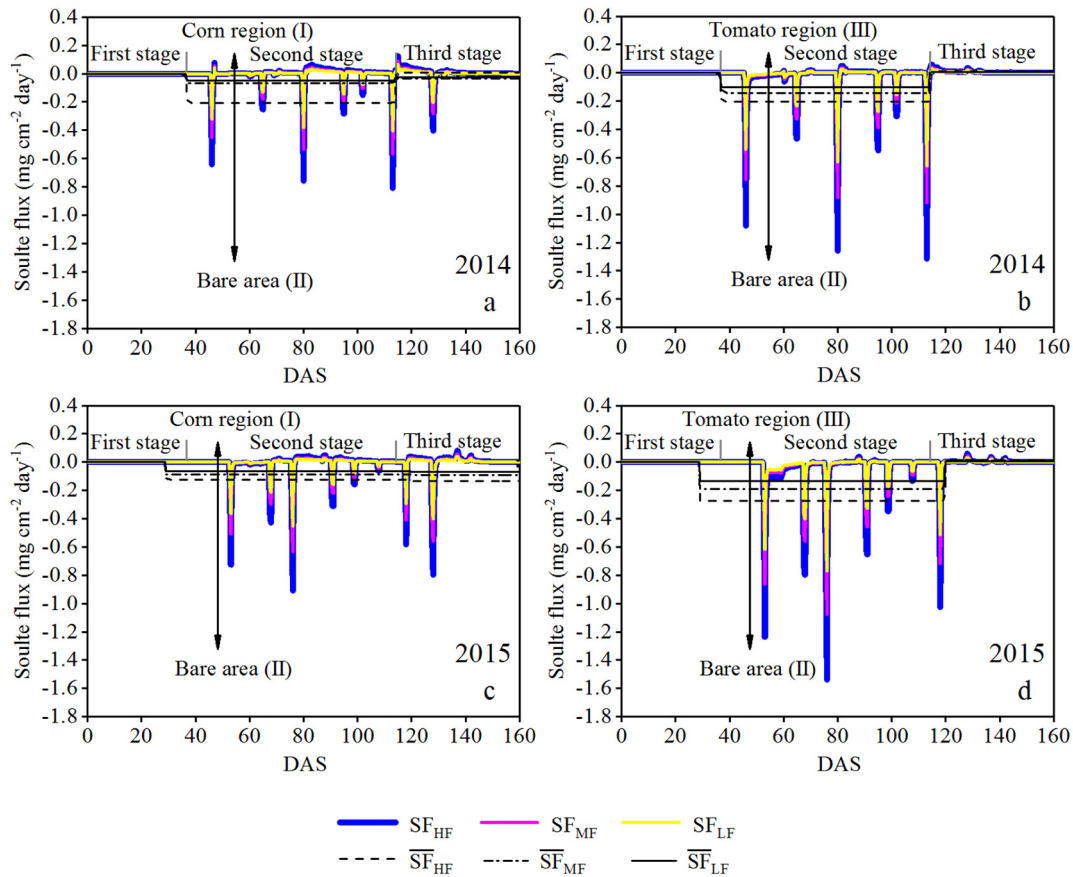
Fig. 6. Simulated soil NO_3-N fluxes in the horizontal direction between the corn (I) and bare (II) regions (left, a and c) and between the tomato (III) and bare (II) regions (right, b and d) during 2014 (top, a and b) and 2015 (bottom, c and d). SF refers to the daily solute flux while $\overline{SF}$ refers to the mean values of the solute flux during different crop stages. Subscripts HF, MF, and LF refer to the high, medium, and low N-fertilizer applications, respectively.

tomato region (III). During the late crop growing season (i.e., during the third stage), large NO_3-N exchange occurred only in the corn region (I) because tomatoes had stopped growing. An average NO_3-N flux from the bare (II) to the corn region (I) was 2.9, 2.0, and 1.5 mg cm^{-1} under HF, MF, and LF in both years, respectively.

3.4. N balance in the root zone of the corn/tomato intercropping ecosystem

Differences in the spatiotemporal ecological functioning of corn and tomato resulted in great differences in the N balance between different root zones of the intercropping ecosystem. The physiological activity of corn was clearly stronger than that of tomato under different N-fertilizer application levels (Fig. 6). N uptake by corn in 2014 and 2015 increased by 38.3% and 42.2%, respectively, compared to tomatoes (Table 6) under the high N-fertilizer application (HF). Additionally, there were significant differences in NO_3-N leaching in the corn and tomato regions. NO_3-N leaching in the corn region in both years was 4.05 and 8.79

times larger than in the tomato region, respectively. First, more N-fertilizer was applied in the corn region, which correspondingly increased NO_3-N leaching in that region. Second, there was intensive NO_3-N exchange in the horizontal direction between different crop regions, while NO_3-N mainly moved from the tomato region (the higher NO_3-N concentration) to the corn region (the lower NO_3-N concentration). As a result, NO_3-N leaching in the tomato region was low. Meanwhile, the soil NO_3-N storage (i.e., Soil$_{end}$) in the root zones of corn and tomato varied widely because of the imbalance in the supply and demand of NO_3-N. The soil NO_3-N storage in the root zone of corn was 51.9% and 52.5% lower than in the tomato region in 2014 and 2015, respectively.

Both N uptake in and NO_3-N leaching from the root zone decreased when an application of the N-fertilizer was reduced by 30% (the medium N-fertilizer application, i.e., MF). N uptake of corn and tomato in both years under MF were 27.7% and 25.6% lower than under HF, while NO_3-N leaching decreased by 37.9% and 54.1%, respectively. When the N-fertilizer application was reduced by 50%, N uptake of

Table 6
Simulated components of the N balance and the N use efficiency (NUE) for corn and tomato under the high (HF), medium (MF), and low (LF) N-fertilizer applications in years 2014 and 2015.

Year	Treatment	Corn					Tomato				
		Applied (kg ha^{-1})	Uptaken (kg ha^{-1})	Leached (kg ha^{-1})	Soil$_{end}$ (kg ha^{-1})	NUE	Applied (kg ha^{-1})	Uptaken (kg ha^{-1})	Leached (kg ha^{-1})	Soil$_{end}$ (kg ha^{-1})	NUE
2014	HF	300.00	222.42	26.43	51.15	0.74	250.00	137.15	6.53	106.32	0.55
	MF	210.00	156.83	18.59	34.58	0.75	175.00	104.08	3.37	67.55	0.59
	LF	150.00	105.14	18.26	26.60	0.70	125.00	63.69	1.39	59.91	0.51
2015	HF	300.00	219.57	21.17	59.27	0.73	250.00	121.67	3.45	124.88	0.49
	MF	210.00	155.75	11.40	42.85	0.74	175.00	88.65	1.39	84.96	0.51
	LF	150.00	105.55	7.06	37.38	0.70	125.00	57.60	0.56	66.84	0.46

corn and tomato in both years were 52.3% and 53.1% lower than under HF, while NO_3-N leaching decreased correspondingly 48.8% and 81.2%, respectively. Additionally, the N use efficiency (NUE) increased nonlinearly with an increase in the N-fertilizer application due to the nonlinearity between the leaf area and N-fertilizer application. For example, the highest NUE can be found for the MF treatment, when it was 3.5% and 9.9% higher than for HF and LF, respectively. Therefore, the MF treatment (210 kg ha^{-1} for corn and 175 kg ha^{-1} for tomato) is suggested to be the optimal fertilization strategy in the corn/tomato intercropping ecosystem.

3.5. Analysis of soil NO_3-N concentrations

Since the NO_3-N movement was consistent for all N-fertilizer application levels, only the NO_3-N behavior in the plot with the high N-fertilizer application (HF) was visually analyzed (Fig. 4). Overall, horizontal differences in SNCs under different crop locations decreased with an increase in the soil depth (Fig. 4). However, SNCs varied widely in the middle between corn rows (P_c), corn and tomato rows (P_b), and tomato rows (P_t) due to differences in applied N-fertilizer amounts, irrigation volumes, and N uptake in the intercropping ecosystem. An obvious difference in SNCs in different horizontal locations (i.e., P_c, P_t, and P_b) can be found in the 0–40 cm soil layer; the difference is highly significant ($P < .01$), especially in the 0–20 cm soil layer. The average SNCs in the 0–20 cm soil layer in both years (2014 and 2015) were 30.9%, and 63.4% higher in P_c and P_t, respectively, compared to P_b during the coexistence period (May–September), while the average SNC in P_t was 29.7% higher than in P_c. As a result, there were large horizontal solute concentration gradients in the shallow soil layer (0–40 cm) in the corn/tomato intercropping ecosystem. On the other hand, there were no significant differences ($P > .05$) in SNCs under different treatments and crop regions in the deep soil layer (40–100 cm) due to intensive N uptake by crops in the shallow soil layer.

4. Discussion

4.1. Soil NO_3-N distribution in an intercropping ecosystem

The distribution of soil NO_3-N in different crop regions of an intercropping ecosystem varied widely due to differences in N uptake capabilities of different crops. Generally, soil NO_3-N concentrations (SNCs) in the region of a crop with higher N uptake were lower than in the region of a crop with lower N uptake. These differences increased in response to an increase in the N-fertilizer application rate (Ojiem et al., 2014; Akanksha et al., 2019). For example, Tsialtas et al. (2018) used the 15N natural abundance method to assess the N competition between the pea and oat and found that the SNC in the oat region was lower than in the pea region of the oat/pea intercropping ecosystem. Similarly, there was a higher SNC in the corn region of the corn/soybean intercropping ecosystem (Chen et al., 2019). Additionally, Ma et al. (2018) indicated that both the root length and distribution of wheat significantly increased, while the corn root growth was suppressed in the wheat/corn intercropping ecosystem. It seems that the crop with stronger root activity absorbs resources from the region of the other crop, which may cause the rooting depth of the crop with stronger root activity to decrease while increasing the rooting depth of the crop with weaker root activity. Overall, the main competition for resources in intercropping ecosystems was concentrated in the 0–40 cm soil layer (Yang et al., 2017; Tian et al., 2018; Chen et al., 2019). Similar results were obtained in this study, with significant differences in SNC found in the 0–40 cm soil layer. The SNC in the corn region decreased on average by 29.7% compared to the tomato region in both years. On the other hand, due to different N-fertilizer applications for different crops in the intercropping ecosystem, larger solute concentration gradients were formed in the horizontal direction, which caused NO_3-N movement from the region with higher solute concentrations to the region with lower solute concentrations (Hillel et al., 1981; Šimůnek and Suarez, 1993). For example, the percentage of N transferred from the pea region with higher solute concentrations to the oat region with lower solute concentrations was between 14.8 and 26.8% (Tsialtas et al., 2018). Similarly, 9.6% of N was transferred from Dalbergia odorifera to Eucalyptus urophylla under the 3 g pot^{-1} urea treatment (Yao et al., 2019). This study similarly revealed that during the stage with an intensive solute exchange, NO_3-N moved in the horizontal direction from the crop region (a high concentration region) to the bare area (a low concentration region) (Fig. 6).

4.2. Soil NO_3-N competition in an intercropping ecosystem

It is important to assess the spatial and temporal N competition between the two crop species to improve field productivity of an intercropping ecosystem (Duan et al., 2019). The difference in N absorption by intercrop species was mainly affected by the root activity, while the crop roots with a stronger activity usually had a relatively strong N uptake capability (Marschner, 2013). For example, Li et al. (2019) studied the N uptake by calla lily in the calla lily/rubber tree intercropping ecosystem. They found that N in the leaves, tubers, and roots of intercropped calla lily was reduced by 11.0%, 20.6%, and 22.6%, respectively. Xie and Kristensen (2016) revealed, based on the analysis of the Relative Competition Index (RCI), that interspecies competition facilitated the growth of leek but hampered that of dyer's woad. Nissen et al. (1999) indicated that although N uptake by cabbage was stronger than that by eucalyptus, the trees can still benefit from the intercropping ecosystem. Similar results were obtained in this study, in which the physiological activity of corn was stronger than that of tomato in the corn/tomato intercropping ecosystem (Fig. 6). Additionally, the nonuniformity of the soil NO_3-N distribution has resulted in differences in N uptake in different root zones of the intercropping ecosystem as well (Fu et al., 2019; Li et al., 2019). For instance, N uptake by corn in 2014 and 2015 increased by 38.3 and 42.2%, respectively, compared to that by tomato, while the SNC in the corn region decreased on average by 29.7% compared with the tomato region in both years (Fig. 4 and Table 6). Similar results were reported by Chen et al. (2019) and Fan et al. (2018), who found that N uptake by corn was higher than by soybean, and the residual NO_3-N in the corn region was lower than in the soybean region.

5. Conclusion

The updated version of HYDRUS-2D capable of considering parameters for two vegetations was used for an intercropping ecosystem. Numerically simulated results showed that soil water contents (SWCs) and soil NO_3-N concentrations (SNCs) were in good agreement with measurements for scenarios with high (300 kg ha^{-1} for corn and 250 kg ha^{-1} for tomato), medium (210 kg ha^{-1} for corn and 175 kg ha^{-1} for tomato), and low (150 kg ha^{-1} for corn and 125 kg ha^{-1} for tomato) N-fertilizer applications (HF, MF, and LF, respectively) during the validation (2015) period. Significant differences in SNCs in the corn, tomato, and bare regions could be found in the 0–40 cm soil layer due to differences in NO_3-N applications to different regions and limited NO_3-N exchange between root zones of different crops. The intensive exchange of NO_3-N in the horizontal direction was found during the second stage (DAS 37-113 in 2014 and DAS 29-120 in 2015). Because of the low soil water potential and soil NO_3-N concentrations gradient between the corn region (I) and the bare area (II), the exchange of NO_3-N between these regions was lower than between the tomato region (III) and the bare area (II). Additionally, NO_3-N leaching in the vertical direction in the corn region was higher than in the tomato region, while N uptake by corn was higher compared to that by tomato. Overall, the results of this study can thus be very useful in designing optimal N-fertilizer applications for intercropped fields.

CRediT authorship contribution statement

Ning Chen: Formal analysis, Investigation, Writing - original draft, Visualization. **Xianyue Li:** Conceptualization, Methodology, Validation, Formal analysis, Resources, Data curation, Writing - review & editing, Visualization, Supervision, Project administration. **Jiří Šimůnek:** Methodology, Software, Data curation, Writing - review & editing. **Haibin Shi:** Data curation, Writing - review & editing. **Qi Hu:** Investigation. **Yuehong Zhang:** Investigation.

Declaration of competing interest

The authors declare that they have no known competing financial interests or personal relationships that could have appeared to influence the work reported in this paper.

Acknowledgments

References

Akanksha, T., Rakesh, K., Rakesh, K., Hardev, R., Meena, R.K., Uttam, K., Yadav, M.R., Subrahmanya, D.J., Adrash, K.P., 2019. Nutritional portfolio of maize and cowpea fodder under various intercropping ratio and balanced nitrogen fertilization. Indian J. Anim. Sci. 89 (3), 276–280.

Allen, R., Pereira, L.S., Raes, D., Smith, M., 1998. Crop Evapotranspiration: Guidelines for Computing Crop Requirements. FAO Irrigation and Drainage Paper No. 56FAO, Rome.

Batista, K., Giacomini, A.A., Gerdes, L., Mattos, W.T.D., Otsuk, I.P., 2019. Impacts of the nitrogen application on productivity and nutrients concentrations of the corn-Congo grass intercropping system in the dry season. Acta Agriculturae Scandinavica, Section B — Soil & Plant Science 69 (7), 567–577.

Bremner, J., Keeney, D., 1965. Steam distillation methods for determination of ammonium, nitrate and nitrite. Anal. Chim. Acta 32, 485–495.

Campbell, G., Norman, J., 1989. The Description and Measurement of Plant Canopy Structure. Plant Canopies: Their Growth Form, and Function. Society for Experimental Biology. Cambridge University Press, Cambridge, pp. 1–19.

Castaldelli, G., Nicolò, C., Tamburini, E., Vincenzi, F., Micòl, M., 2018. Soil type and microclimatic conditions as drivers of urea transformation kinetics in maize plots. Catena 166, 200–208.

Chen, P., Song, C., Liu, X.M., Zhou, L., Yang, H., Zhang, X., Zhou, Y., Du, Q., Pang, T., Fu, Z.D., Wang, X.C., Liu, W.G., Yang, F., Shu, K., Du, J., Liu, J., Yang, W., Yong, T., 2019. Yield advantage and nitrogen fate in an additive maize-soybean relay intercropping system. Sci. Total Environ. 657, 987–999.

Cichota, R., Vogeler, I., Snow, V., Shepherd, M., Mcauliffe, R., Welten, B., 2018. Lateral spread affects nitrogen leaching from urine patches. Sci. Total Environ. 635, 1392–1404.

Cote, C., Bristow, K., Charlesworth, P., Cook, F., Charlesworth, P., 2003. Analysis of soil wetting and solute transport in subsurface trickle irrigation. Irrig. Sci. 22 (3–4), 143–156.

Cruz, I.L., Aguilar, A.R., Raquel, S.M., López, R.L., 2014. Global sensitivity analysis of crop growth sucros model applied to husk tomato. Revista fitotecnia mexicana publ 37 (3), 279–288.

Das, P.C., Kamble, S.P., Velmurugan, P., Pradhan, D., 2019. Evaluation of minor carps intercropping in carp polyculture vis-a-vis other grow-out cropping patterns of carp farming. Aquac. Res. 50 (6), 1574–1584.

Ding, L., Jin, Y.Z., Li, Y.H., Wang, Y.B., 2014. Spatial pattern and water-saving mechanism of wheat and maize under the condition of strip-ridge intercropping. A Acta Agric. Boreali-Occident. Sin. 23 (6), 56–63.

Du, B., Pang, J., Hu, B., Allen, D.E., Bell, T.L., Pfautsch, S., Netzer, F., Dannenmann, M., Zhang, S., Rennenberg, H., 2019. N_2-fixing black locust intercropping improves ecosystem nutrition at the vulnerable semi-arid Loess Plateau region, China. Sci. Total Environ. 688, 333–345.

Duan, Y., Shen, J.Z., Zhang, X.L., Wen, B., Ma, Y.C., Wang, Y.H., Fang, W.P., Zhu, X.J., 2019. Effects of soybean–tea intercropping on soil-available nutrients and tea quality. Acta Physiol. Plant. 41 (8).

Elasbah, R., Selim, T., Mirdan, A., Berndtsson, R., 2019. Modeling of fertilizer transport for various fertigation scenarios under drip irrigation. Water 11 (5), 893.

Fan, Y.W., Gong, J.G., Wang, Y., Shao, X.X., Zhao, T., 2018. Application of Philip infiltration model to film hole irrigation. Water Supply 19 (3), 978–985.

Feddes, R., Kowalik, P., Zaradny, H., 1978. Simulation of Field Water Use and Crop Yield. John Wiley & Sons, New York.

Filipović, V., Coquet, Y., Pot, V., Houot, S., Benoit, P., 2014. Modeling the effect of soil structure on water flow and isoproturon dynamics in an agricultural field receiving repeated urban waste compost application. Sci. Total Environ. 499, 546–559.

Fu, Z.D., Zhou, L., Chen, P., Du, Q., Pang, T., Song, C., Wang, X.C., Liu, W.G., Yang, W.Y., Yong, T., 2019. Effects of maize-soybean relay intercropping on crop nutrient uptake and soil bacterial community. J.of Integr. Agric. 18 (9), 2006–2018.

Gao, Y., Duan, A.W., Qiu, X.Q., Liu, Z.G., Sun, J.S., 2010. Distribution of roots and root length density in a maize/soybean strip intercropping system. Agric. Water Manag. 98 (1), 199–212.

Grecco, K.L., Miranda, J.H., Silveira, L.K., van Genuchten, M.T., 2019. HYDRUS-2D simulations of water and potassium movement in drip irrigated tropical soil container cultivated with sugarcane. Agric. Water Manag. 221, 334–347.

Hanson, B., Šimůnek, J., Hopmans, J., 2006. Evaluation of urea–ammonium–nitrate fertigation with drip irrigation using numerical modeling. Agric. Water Manag. 86 (1–2), 102–113.

Hartmann, T.E., Yue, S.C., Schulz, R., He, X.K., Chen, X.P., Zhang, F.S., Müller, T., 2015. Yield and N use efficiency of a maize–wheat cropping system as affected by different fertilizer management strategies in a farmer's field of the North China plain. Field Crops Res 174, 30–39.

Hauggaard, N.H., Lachouani, P., Knudsen, M.T., Ambus, P., Boelt, B., Gislum, R., 2016. Productivity and carbon footprint of perennial grass–forage legume intercropping strategies with high or low nitrogen fertilizer input. Sci. Total Environ. 541, 1339–1347.

He, Q.S., Li, S.E., Kang, S.Z., Yang, H.B., Qin, S.J., 2018. Simulation of water balance in a maize field under film-mulching drip irrigation. Agric. Water Manag. 210, 252–260.

Hillel, D., 1981. Soil and water, physical principles and processes. Agricultural Press https://doi.org/10.1016/b978-0-124-77915-0.x5001-5 Beijing.

Hu, F., Gan, Y., Chai, Q., Feng, F., Zhao, C., Yu, A., Mu, Y., Zhang, Y., 2016. Boosting system productivity through the improved coordination of interspecific competition in maize/pea strip intercropping. Field Crops Res 198, 50–60.

Iqbal, N., Hussain, S., Ahmed, Z., Yang, F., Wang, X., Liu, W., Yong, T., Du, J., Shu, K., Yang, W., Liu, J., 2019. Comparative analysis of maize–soybean strip intercropping systems: a review. Plant Prod. Sci. 22 (2), 131–142.

Karandish, F., Šimůnek, J., 2018. An application of the water footprint assessment to optimize production of crops irrigated with saline water: a scenario assessment with HYDRUS. Agric. Water Manag. 208, 67–82.

Li, X.Y., Shi, H.B., Šimůnek, J., Gong, X.W., Peng, Z.Y., 2015a. Modeling soil water dynamics in a drip-irrigated intercropping field under plastic mulch. Irrig. Sci. 33 (4), 289–302.

Li, Y., Šimůnek, J., Zhang, Z., Jing, L., Ni, L., 2015b. Evaluation of nitrogen balance in a direct-seeded-rice field experiment using Hydrus-1D. Agric. Water Manag. 148, 213–222.

Li, X.Y., Šimůnek, J., Shi, H.B., Yan, J.W., Peng, Z.Y., Gong, X.W., 2017. Spatial distribution of soil water, soil temperature, and plant roots in a drip-irrigated intercropping field with plastic mulch. Eur. J. Agron. 83, 47–56.

Li, J., Xie, R.Z., Wang, K.R., Hou, P., Ming, B., Zhang, G.Q., Ming, B., Zhang, G.Q., Liu, G.Z., Wu, M., Yang, Z.S., Li, S.K., 2018. Response of canopy structure, light interception and grain yield to plant density in maize. J. Agric. Sci. 156 (6), 785–794.

Li, J., Zhou, L.J., Lin, W.F., 2019. Calla lily intercropping in rubber tree plantations changes the nutrient content, microbial abundance, and enzyme activity of both rhizosphere and non-rhizosphere soil and calla lily growth. Ind. Crop. Prod. 132, 344–351.

Liu, J., Bi, X.Q., Ma, M.T., Jiang, L.H., Du, L.F., Li, S.J., Sun, Q.P., Zou, G.Y., Liu, H.B., 2019. Precipitation and irrigation dominate soil water leaching in cropland in Northern China. Agric. Water Manag. 211, 165–171.

Ma, L., Li, Y., Wu, P., Zhao, X., Chen, X., Gao, X., 2018. Effects of varied water regimes on root development and its relations with soil water under wheat/maize intercropping system. Plant Soil 439 (1–2), 113–130.

Marschner, P., 2013. Marschner's Mineral Nutrition of Higher Plants. Second edition. Science Press.

Martin, G.M.O., Paquette, A., Dupras, J., Rivest, D., 2018. The new green revolution: sustainable intensification of agriculture by intercropping. Sci. Total Environ. 615, 767–772.

Nissen, T.M., Midmore, D.J., Cabrera, M.L., 1999. Aboveground and belowground competition between intercropped cabbage and young Eucalyptus torelliana. Agrofor. Syst. 46, 83–93.

Noulas, C., Herrera, J.M., Tziouvalekas, M., Qin, R.J., 2018. Agronomic assessment of nitrogen use efficiency in spring wheat and interrelations with leaf greenness under field conditions. Commun. Soil Sci. Plant Anal. 49 (5–7), 763–781.

Ojiem, J.O., Franke, A.C., Vanlauwe, B., De Ridder, N., Giller, K.E., 2014. Benefits of legume–maize rotations: assessing the impact of diversity on the productivity of smallholders in western Kenya. Field Crops Res 168, 75–85.

Rai, V., Pramanik, P., Das, T.K., Aggarwal, P., Bhattacharyya, R., Krishnan, P., Sehgal, V.K., 2019. Modelling soil hydrothermal regimes in pigeon pea under conservation agriculture using Hydrus-2D. Soil Tillage Res. 190, 92–108.

Ramos, T., Šimůnek, J., Gonçalves, M., Martins, J., Prazeres, A., Pereira, L., 2012. Two-dimensional modeling of water and nitrogen fate from sweet sorghum irrigated with fresh and blended saline waters. Agric. Water Manag. 111, 87–104.

Ravikumar, V., Vijayakumar, G., Šimůnek, J., Chellamuthu, S., Santhi, R., Appavu, K., 2011. Evaluation of fertigation scheduling for sugarcane using a vadose zone flow and transport model. Agric. Water Manag. 98, 1431–1440.

Raza, M.A., Bin Khalid, M.H., Zhang, X., Feng, L.Y., Khan, I., Hassan, M.J., Ahmed, M., Ansar, M., Chen, Y.K., Fan, Y.F., Yang, F., Yang, W., 2019a. Effect of planting patterns on yield, nutrient accumulation and distribution in maize and soybean under? Relay intercropping systems. Sci. Rep. 9 (1), 4947.

Raza, S., Chen, Z.J., Ahmed, M., 2019b. Dicyandiamide application improved nitrogen use efficiency and decreased nitrogen losses in wheat-maize crop rotation in Loess Plateau. Arch. Agron. Soil Sci. 65 (4), 450–464.

Ren, J., Wang, X.P., Shen, Z.Z., Zhao, J., Yang, J., Ye, M., Zhou, Y.Y., Wang, Z.H., 2018. Heat tracer test in a riparian zone: laboratory experiments and numerical modelling. J. Hydrol. 563, 560–575.

Skaggs, T.H., Trout, T.J., J, Šimunek, Shouse, P.J., 2004. Comparison of Hydrus-2D simulations of drip irrigation with experimental observations. J Irrig Drain Eng 130 (4), 304–310.

Scalise, A., Pappa, V.A., Gelsomino, A., Rees, R.M., 2017. Pea cultivar and wheat residues affect carbon/nitrogen dynamics in pea-triticale intercropping: a microcosms approach. Sci. Total Environ. 592, 436–450.

Schaap, M., Leij, F., van Genuchten, M.Th, 2001. ROSETTA: a computer program for estimating soil hydraulic parameters with hierarchical pedotransfer functions. J. Hydrol. 251, 163–176.

Simone, D.P., Mirko, C., Majdi, R.A.N., Ryan, D.S., Rafael, A.J., Thierry, W., Laurent, L., 2019. Experimental assessment of a new comprehensive model for single ring infiltration data. J. Hydrol. 573, 937–951.

Šimůnek, J., Hopmans, J.W., 2009. Modeling compensated root water and nutrient uptake. Ecol. Model. 220 (4), 505–521.

Šimůnek, J., Suarez, D.L., 1993. Modeling of carbon dioxide transport and production in soil: 1. Model development. Water Resour. Res. 29 (2), 487–497. https://doi.org/10.1029/92wr02225.

Šimůnek, J., van Genuchten, M.T., Šejna, M., 2016. Recent developments and applications of the HYDRUS computer software packages. Vadose Zone J. 15, 25.

Singh, B., Aulakh, C.S., Walia, S.S., 2017. Productivity and water use of organic wheat–chickpea intercropping system under limited moisture conditions in northwest India. Renewable Agriculture and Food Systems 1–10.

Streit, J., Meinen, C., Nelson, W.C.D., 2019. Above- and belowground biomass in a mixed cropping system with eight novel winter faba bean genotypes and winter wheat using FTIR spectroscopy for root species discrimination. Plant Soil 436 (1–2), 141–158.

Sun, T., Li, Z.Z., Wu, Qi., Sheng, T.T., Du, M.Y., 2018. Effects of alfalfa intercropping on crop yield, water use efficiency, and overall economic benefit in the Corn Belt of Northeast China. Field Crops Res 216, 109–119.

Tafteh, A., Sepaskhah, A., 2012. Application of HYDRUS-1D model for simulating water and nitrate leaching from continuous and alternate furrow irrigated rapeseed and maize fields. Agric. Water Manag. 113, 19–29.

Tian, X., Li, C., Zhang, M., Li, T., Lu, Y., Liu, L., 2018. Controlled release urea improved crop yields and mitigated nitrate leaching under cotton-garlic intercropping system in a 4-year field trial. Soil Tillage Res. 175, 158–167.

Tsialtas, I.T., Dimitrios, B., Vlachostergios, D.N., Christos, D., Anastasios, L., 2018. Cultivar complementarity for symbiotic nitrogen fixation and water use efficiency in pea-oat intercrops and its effect on forage yield and quality. Field Crop Res. 226, 28–37.

Wang, H., Ju, X., Wei, Y., Li, B., Zhao, L., Hu, K., 2010. Simulation of bromide and nitrate leaching under heavy rainfall and high-intensity irrigation rates in North China Plain. Agric. Water Manag. 97, 1646–1654.

Wang, Y., Zhang, B., Lin, L., Zepp, H., 2011. Agroforestry system reduces subsurface lateral flow and nitrate loss in Jiangxi province, China. Agri. Eco. Envir. 140 (3–4), 441–453.

Wang, X.K., Wang, N., Xing, Y.Y., Mohamed, B.E.C., 2018. Synergetic effects of plastic mulching and nitrogen application rates on grain yield, nitrogen uptake and translocation of maize planted in the Loess Plateau of China. Sci. Rep. 8 (1), 14319.

Wesseling, J.G., Brandyk, T., 1985. Introduction of the Occurrence of High Groundwater Levels and Surface Water Storage in Computer Program SWATRE, Nota 1636. Institute for Land and Water Management Research (ICW), Wageningen, The Netherlands.

Xie, Y., Kristensen, H.L., 2016. Intercropping leek (allium porrum l.) with dyer's woad (isatis tinctoria l.) increases rooted zone and agro-ecosystem retention of nitrogen. Eur. J. Agron. 82, 21–32.

Xu, C.D., Tian, J.J., Wang, G.X., Nie, J.K., Zhang, H.Y., 2019. Dynamic simulation of soil salt transport in arid irrigation areas under the HYDRUS-2D-based rotation irrigation mode. Water Res. Manage. 33 (10), 3499–3512.

Yang, L.L., Ding, X.Q., Liu, X.J., Li, P.M., Eneji, E., 2016. Impacts of long-term jujube tree/winter wheat–summer maize intercropping on soil fertility and economic efficiency—a case study in the lower North China Plain. Eur. J. Agron. 75, 105–117.

Yang, F., Liao, D., Wu, X., Gao, R., Fan, Y., Raza, M.A., et al., 2017. Effect of aboveground and belowground interactions on the intercrop yields in maize-soybean relay intercropping systems. Field Crop Res. 203, 16–23 (Complete).

Yao, X.Y., Li, Y.F., Liao, L.N., Sun, G., Wang, H.X., Ye, S.M., 2019. Enhancement of nutrient absorption and interspecific nitrogen transfer in a Eucalyptus urophylla × eucalyptus grandis and Dalbergia odorifera mixed plantation. Forest Eco. Mange. 449, 117465.

Zhao, Y.H., Fan, Z.L., Hu, F.L., Yin, W., Zhao, C., Yu, A.Z., Chai, Q., 2019. Source-to-sink translocation of carbon and nitrogen is regulated by fertilization and plant population in maize-pea intercropping. Front. Plant Sci. 10, 891.

Zhou, T., Wang, L., Yang, H., Gao, Y., Liu, W.G., Yang, W.Y., 2019. Ameliorated light conditions increase the P uptake capability of soybean in a relay-strip intercropping system by altering root morphology and physiology in the areas with low solar radiation. Sci. Total Environ. 688, 1069–1080.